INTERNATIONAL JOURNAL OF POLYMERIC MATERIALS AND POLYMERIC BIOMATERIALS
2018, VOL. 67, NO. 12, 745–753
https://doi.org/10.1080/00914037.2017.1376201



# Influence of antistatic agent encapsulated into functionalized mesoporous silica on antistatic properties of polystyrene

Jingjing Si[a,b] and Ping Tang[a]

[a]State Key Laboratory of Molecular Engineering of Polymers, Department of Macromolecular Science, Fudan University, Shanghai, China; [b]College of Civil and Transportation Engineering, Hohai University, Nanjing, Jiangsu, China

**ABSTRACT**

Small molecular surfactant (SMS) such as HDC-193 was encapsulated into mesoporous silica SBA-15 and 3-aminopropyltriethoxysilane-modified SBA-15 (mSBA-5) to develop new controlled release SMS system. The diffusion process of HDC-193 from mesoporous silica with different structures and diameters was investigated. Both situations of large pore and organic modification promoted the adsorption and thus a larger load of SMS in mesoporous silica. The results of molecular dynamics simulations and washing durability experiments showed that the lifetime of HDC-193 encapsulated into mSBA-15 in polystyrene blends is five times longer than that of HDC-193/polystyrene. This suggests an efficient strategy for designing permanent antistatic agents.

**GRAPHICAL ABSTRACT**

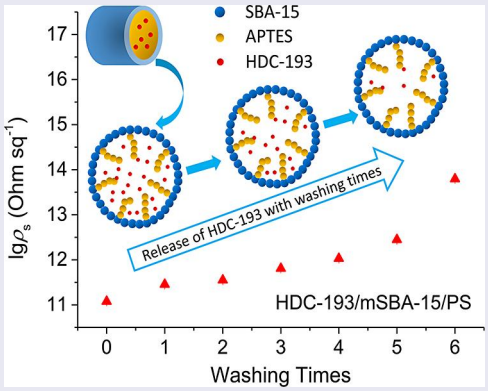


**ARTICLE HISTORY**
Received 6 June 2017
Accepted 2 September 2017

**KEYWORDS**
Antistatic agent; antistatic property; mesoporous silica; polystyrene; washing durability

## 1. Introduction

Electrostatic charges are prone to accumulate on the surface of most of the polymers, which is a serious technological problem responsible for shocks and explosions [1,2] as well as damage to satellites [3] and other electronic equipment measured in billions of dollars costs each year [4]. Static electricity is generated whenever two insulating materials touch and then separate. One material charges positively, and the other charges negatively. Despite centuries of research, it is still not known why certain polymers charge more than others and, most importantly, how to design polymers that would resist static electricity. Works by Baytekin et al. [5,6], Burgo et al. [7], and Williams [8] revealed that electrification of polymers due to physical contact leads to spatially heterogeneous transfer of charge and material as well as the creation of radicals upon homolytic bond cleavage [9].

Antistatic polymers are generally prepared by blending polymer matrices with antistatic agents, allowing the formation of new polymeric materials with the magnitude of volume electrical resistivity ($\rho_v$) lower than $10^{13}\,\Omega$ cm or surface electrical resistivity ($\rho_s$) lower than $10^{12}\,\Omega\,sq^{-1}$ [10,11]. The antistatic agents are usually conductive material or small molecular surfactant (SMS). The conductive materials, e.g., metal filler, [12,13] inorganic nonmetallic fillers [14–16] and conductive polymers, which have relatively homogeneous and stable electrical properties, [17–20] can dissipate charges by building internal percolation conductive network. However, a large amount of the conductive materials in a polymer matrix is usually required (above 5 wt%) to form the internal conductive network and achieve high electrical conductivity [21]. This may deteriorate other physical properties of composites, such as optical transparency

**CONTACT** Ping Tang pingtang@fudan.edu.cn State Key Laboratory of Molecular Engineering of Polymers, Department of Macromolecular Science, Fudan University, Shanghai 200433, China.
Color versions of one or more of the figures in the article can be found online at www.tandfonline.com/gpom.

[21–26], mechanical properties, and viscosity [27], thus limiting the application of these polymers. The SMS is widely used as antistatic agent in industry, because a small amount of the SMS (about 1–3 wt%) is required to effectively improve the antistatic property of polymer matrix. The SMS is amphipathic small molecule which can easily migrate from the interior to the surface of polymer and adsorb moisture from the surrounding air, resulting in the reduction of the surface electrostatic charges [28]. However, the SMS can be easily washed out and consumed due to its quickly migrating to the polymer surfaces, and consequently decreasing the lifetime of SMS [29].

In the previous work, the SMS HDC-102 and HDC-193 have been encapsulated into channels of mesoporous silica nanoparticles to obtain controllable migration rate and enhance the lifetime of SMS [30], The small molecules with controllable migration rate have recently attracted intensive research for various applications, such as packaging [31,32], additive migration, gas separation [33,34], osmosis [35,36], biosensors [37], drug releases [38,39], ion exchange, and so on [40]. In these research fields, mesoporous materials (e.g., mesoporous $SiO_2$, mesoporous $Fe_3O_4$, mesoporous carbon and polymer with mesoporous framework) are usually adopted as carriers for small molecules [41]. Recently, this strategy has been applied in designing antistatic agent to achieve efficient and durable antistatic polymers [30]. The mesoporous silica MCM-41 was used as the carrier to control the migration of SMS in polystyrene (PS) matrix, thereby enhancing the lifetime of SMS.

The adsorption and release process of small molecules can be controlled by tailoring the composition, pore configuration, and surface performances of mesoporous materials, thereby mesoporous silica and its organic-modified analogues have been tried in the delivery of drugs [42]. However, how the pore size and functionalization of mesoporous silica influence the accommodation and release of the SMS is still inexplicit and detailed study is required. For this purpose, molecular dynamics (MD) simulations were used here to predict the effects of pore size of mesoporous silica on SMS diffusion rate. Under this guidance, the mesoporous silica SBA-15 was modified by positively charged amino groups to promote the adsorption of mesoporous silica to SMS and thus prolonging the release time of SMS from the inner mesoporous silica to the PS composite surface.

## 2. Experiments

### 2.1. Materials

The mesoporous silica SBA-15 and MCM-41 were purchased from Nanjing XFNANO Materials Tech Co., Ltd. The ionic SMS HDC-193 with 95% effective mass content was purchased from Hangzhou Lin'an Dechang Electrostatic Technology Co., Ltd. The PS with the $\overline{M}_w$ of $2.58 \times 10^5$ g mol$^{-1}$ was purchased from Aladdin. The 3-aminopropyltriethoxysilane (APTES) was purchased from J&K Scientific Ltd. The ethanol and xylene with analytical pure were purchased from Aladdin and were used as received.

### 2.2. Sample preparation

#### 2.2.1. Preparation of functionalized mesoporous silica

The SBA-15 was dried in vacuum oven at 80°C for 24 h to remove the adsorbed water. The dried SBA-15 2.0 g was dispersed in 100 mL of ethanol in 250-mL flask (20 mg mL$^{-1}$), with ultrasonication for 30 min. A total of 2.0 g of APTES was dissolved in ethanol (20 wt%) and then added into the SBA-15 dispersion with stirring and refluxing for 12 h. Finally, the mixture was filtered, washed with about 100 mL of ethanol, and dried in vacuum oven at 50°C for about 24 h to obtain the APTES-modified mesoporous silica mSBA-15.

#### 2.2.2. Encapsulating of SMS in functionalized mesoporous silica

The ionic SMS HDC-193 was dried in vacuum oven at 45°C for 48 h to remove the adsorbed water. First, 2.0 g of SMS was dissolved in ethanol (33 mg mL$^{-1}$) with ultrasonication for 30 min. Then, 1.0 g of mSBA-15 was added, stirring for 48 h, and preventing the evaporation of ethanol. After that, the mixture was filtered and the cake was washed more than thrice by ethanol (about 200 mL) to remove the surfactant molecules attached on the surface of mSBA-15. Finally, the cake was dried by vacuum freeze-drying to obtain the encapsulated antistatic agents HDC-193/mSBA-15. To make comparison, the HDC-193/SBA-15 was prepared with the same method.

#### 2.2.3. Preparation of polystyrene composite

The PS composites were prepared through solution cast technique [43,44]. A predetermined weight of the encapsulated antistatic agent in xylene (the concentration of mixed solution was 20 wt%) was first ultrasonicated for 30 min. The PS (5.0 g) was added into the encapsulated antistatic agent dispersion and stirred for 3 h at room temperature. The viscous solution was casted into glass culture dish, followed by programmed drying in vacuum oven at 100°C/0.5 h + 120°C/6 h to obtain a series of PS composites with different HDC-193 weight fractions (0.5, 1.0, 1.5, and 2.0%).

To test the surface electrical resistivity $\rho_s$, the PS composite disk with diameter of about 10 cm and thickness of about 1 mm was obtained. The plate vulcanizing machine (QLB-D, China) and the molds were preheated to 185°C. Then the PS composite was put in the mold and pressed at 185°C for 5 min with a pressure of 10 MPa in plate vulcanizing machine, followed by cold pressing of 10 MPa for about 1 min in another plate vulcanizing machine and then demolding.

### 2.3. Characterization

#### 2.3.1. Infrared spectroscopy

Infrared (IR) spectra of the samples were recorded from samples pressed into pellets with KBr powder using a NEXUS 470 FTIR spectrometer (Thermo Fisher, USA). The transition mode was used and the wavenumber ranged from 4000 to 500 cm$^{-1}$.

#### 2.3.2. Nuclear magnetic resonance

Nuclear magnetic resonance (NMR) $^{1}H$ NMR and $^{13}C$ NMR spectra of HDC-193 were obtained by a Bruker (500 MHz) NMR instrument, using $CDCl_3$ as the solvent and tetramethylsilane as the interior reference.

#### 2.3.3. Matrix-assisted laser desorption/ionization time-of-flight mass spectrometry

Matrix-assisted laser desorption/ionization time-of-flight mass spectrometry (MALDI-TOF MS) was performed on Voyager DE-STR MALDI-TOF MS instrument equipped with a 337-nm nitrogen laser. Samples, dithranol (matrix) and silver trifluoroacetate were dissolved in tetrahydrofuran with the concentrations of 10, 20, and 10 mg $mL^{-1}$, respectively. These solutions were mixed in the volume ratio of matrix:sample:salt = 10:2:1. A volume of 0.5 μL of the mixed solution was placed on a copper plate and air-dried at ambient temperature. Mass spectra were acquired in positive reflector mode using an acceleration voltage of 25 kV.

#### 2.3.4. Morphological characterization

The field emission scanning electron microscopy (FE-SEM) image of mSBA-15 was recorded on an Ultra 55 FE-SEM (Zeiss, Germany). The atomic force microscopy (AFM) images of PS composites were performed using a Multimode 8 AFM (Bruker, USA). All measurements were made at ambient temperature. Moreover, intermediate to hard tapping mode was used to reveal good contrast in both height and phase images.

#### 2.3.5. Particle surface and size characterization

Nitrogen gas ($N_2$) adsorption/desorption isotherms were measured at 77 K using a Micromeritics Tristar 3000 instrument, with the samples pre-heated in vacuum at 348 K for 12 h. The surface area of samples was measured using the Brunauer–Emmett–Teller (BET) method and the pore size data were analyzed with the thermodynamic-based Barrett–Joyner–Halenda method based on the adsorption and desorption branches of the $N_2$ isotherm [45,46].

#### 2.3.6. Thermogravimetric analysis

Thermogravimetric analysis (TGA, Pyris 1, PE Instrument, USA) was conducted under $N_2$ atmosphere with the flow rate of 40 mL $min^{-1}$ from ambient temperature to 800°C at a heating rate of 20°C $min^{-1}$.

#### 2.3.7. Surface electrical resistivity

The $\rho_s$ of the PS and its composites was measured through a Keithley 6517B Electrometer (USA) in ambient [relative humidity (RH): 55 ± 5%]. The thickness of specimen, test voltage, and bias holding time were about 1 mm, 500 V, and 1 min, respectively.

#### 2.3.8. Washing durability

The washing durability of the sheet samples was evaluated by comparing the $\rho_s$ before and after washing. The samples were immersed in a flask (250 mL) with ~200 mL of deionized water and ultrasonicated for 30 min and then dried in air at 23°C, 60% RH for 24 h [21].

### 2.4. Molecular dynamics simulations

The large-scale atomic/molecular massively parallel simulator code was used to simulate the diffusion process of SMS in PS matrix. The MD simulations were performed in the microcanonical ensemble (NVE) with a time step of 0.01 ps. The locations of SMS were recorded every 1000 steps (10 ps). The simulation results were visualized by visual molecular dynamics.

Based on the molecular structure of PS, SMS, and mesoporous silica nanoparticle (MSN), particles with different polarity were used which denote the segment and functional groups. The PS molecular chain was constituted by 100 styrene particles, and there were 500 PS molecular chains in the system. There were 50 SMS molecules in the system, which was constituted by three particles which denoted $-CH_2-CH_2-CH_2-$ structure, ester group, and hydroxyl group, respectively. The MSN was denoted as a hollow cylinder. In the PS composite with encapsulated antistatic agent, the MSN with varied inside radius ($r = 2$, 4, and 6 units, respectively) was introduced and fixed in the system, which was named as SMS/MSN/PS2, SMS/MSN/PS4, and SMS/MSN/PS6.

The diffusion coefficient ($D_G$) of SMS was calculated according to Eq. 1:

$$\mathrm{MSD} = 6D_G t \tag{1}$$

where MSD is the mean-square displacement of SMS, $t$ is the simulation time.

## 3. Results and discussion

### 3.1. Structures of functionalized mesoporous silica

The mesoporous silica SBA-15 was modified by APTES, and the functional groups, pore size, and morphology of SBA-15 and mSBA-15 were characterized. Figure 1a shows the FE-SEM image of SBA-15, from which the nanoparticles with rod-like shapes can be seen. The mesoporous silica was composed of Si–O–Si structure, which showed the peak in 1080 $cm^{-1}$ in the FTIR spectrum of SBA-15 (Figure 1b). For mSBA-15, the N–H and C–H structures were assigned at 3440 and 2929 $cm^{-1}$, respectively, which were the feature structures of APTES. The characteristic absorption band at 1080 $cm^{-1}$ (Si–O–Si) was obviously strengthened after SBA-15 being modified by APTES (Figure 1b), indicating that the C–O–Si groups of APTES C–O–Si reacted with Si–OH on the surface and in the channel of SBA-15 particles through transesterification.

The measured $N_2$ adsorption/desorption isotherms and calculated pore diameter distribution of SBA-15 and mSBA-15 are shown in Figures 1c and 1d. According to Figure 1c, functionalization with amine organosiliane APTES did not change the mesoporous structure. From the special point of relative pressure $P/P_0$ at which the capillary condensation occurs, it can be found that this point decreased from 0.6 (SBA-15) to 0.4 (mSBA-15), which indicated the reduced pore diameter caused by APTES modifying the channels of SBA-15. The SBA-15 showed uniform, ordered pores with an average diameter $d_{BJH}$ of 6.39 nm and the largest pore diameter

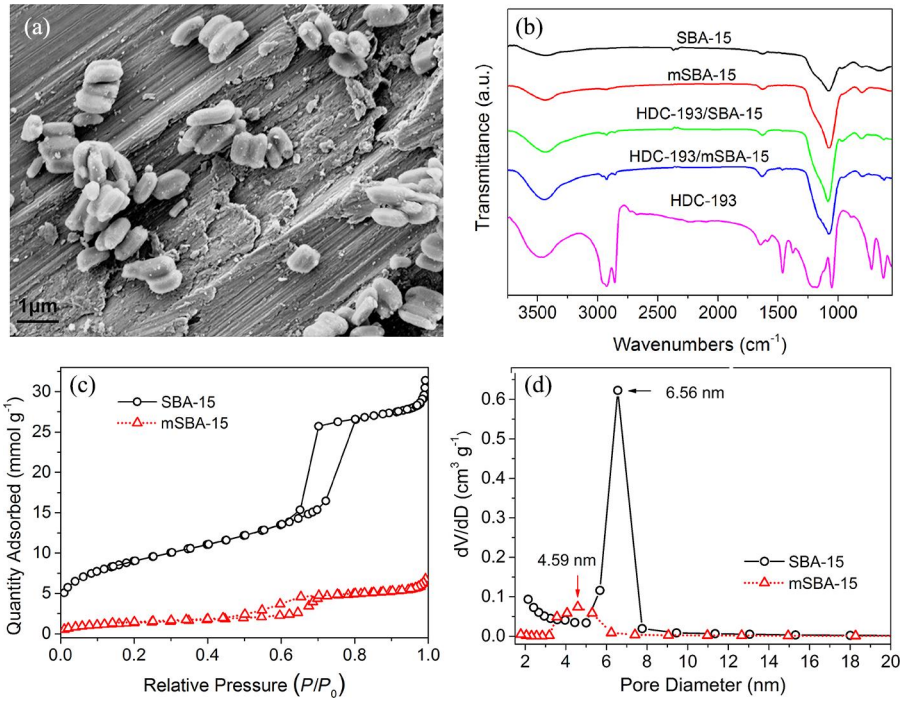


**Figure 1.** (a) SEM image of SBA-15, (b) FTIR spectra of HDC-193, SBA-15, mSBA-15, HDC-193/SBA-15, and HDC-193/mSBA-15, (c, d) $N_2$ adsorption/desorption isotherm and pore diameter distribution of SBA-15 and mSBA-15. *Note*: SEM, scanning electron microscopy.

$d_{BJH\ Max}$ of 6.56 nm (Figure 1d). The $d_{BJH}$ and $d_{BJH\ Max}$ of mSBA-15 decreased to 6.14 and 4.59 nm, indicating the smaller pore size caused by the introduction of organic groups into channels. The mSBA-15 particle has smaller BET surface area ($S_{BET}$, 112.99 $m^2\,g^{-1}$) and pore volume ($V_{BJH}$, 0.24 $cm^3\,g^{-1}$) than that of SBA-15 (726.31 $m^2\,g^{-1}$ and 1.13 $cm^3\,g^{-1}$, respectively).

### 3.2. Structures of small molecular surfactants

The HDC-193 is anionic surfactant, which is an antistatic agent for PS. The molecular structure of HDC-193 was characterized through FTIR. In the FTIR spectrum of HDC-193, several peaks at 1591, 1464, 1377, and 1192 $cm^{-1}$ indicated alkylene group, peaks at 3466, 1645, and 1464 $cm^{-1}$ indicated carboxyl group (Figure 1b). As a result, the HDC-193 contains unsaturated aliphatic chain and carboxylate.

The structure of HDC-193 was confirmed by $^1H$ NMR, $^{13}C$ NMR (Figures 2a and 2b), and MALTDI-TOF spectrum (Figure 2c). Analysis of the HDC-193 by $^1H$ NMR and $^{13}C$ NMR revealed unsaturated aliphatic chain and carboxylate. The ratio of proton peak area at $\delta = 0.90$ ppm to peak area at $\delta = 1.27$ ppm was 1:0.31, indicating that the ratio of $-CH_3$ to $-CH_2-$ was 1:5.

According to the MALTDI-TOF spectrum (Figure 2c), there were $-CH_3$, $-CH_2-$, –COO, and methylbenzene molecular fragments in the HDC-193. Moreover, there were molecular fragments in 400–1000 *m/z*, which might be PS oligomers. Based on the analysis of FTIR, NMR, and MALTDI-TOF spectra, the HDC-193 was consisted with PS oligomer and anionic. The chemical structure of anionic was speculated and is shown in Figure 2d.

### 3.3. Effective SMS uptake of functionalized mesoporous silica

The effective SMS uptakes of SBA-15 and mSBA-15 were monitored by TGA (Figure 3a). The content ($C$) of SMS encapsulated in SBA-15 or mSBA-15 was calculated according to Eq. 2:

$$C = \frac{W_{MSN} - W_{COM}}{W_{MSN} - W_{SMA}} \quad (2)$$

where $W_{MSN}$, $W_{COM}$, and $W_{SMA}$ are weight residues at 700°C for SBA-15 or mSBA-15, SMS/SBA-15, and SMS, respectively. For SBA-15, $W_{MSN} = 1$, for mSBA-15, $W_{MSN} < 1$. The $C$ values of HDC-193 in SBA-15 and mSBA-15 are shown in Figure 3b. To compare the effective SMS uptake of different pore diameters of mesoporous silica, the TGA curves of HDC-193/MCM-41 and HDC-193/mMCM-41 are shown in Figure 3b and the $C$ values were calculated according to Eq. 2.

The $C$ values were increased with the pore diameter, while too large pore diameter was negative for SMS encapsulating. The pore diameter sequence of mesoporous silica was SBA-15 > mSBA-15 > MCM-41 > mMCM-41, and the $C$ value of HDC-193 encapsulated in these mesoporous silica was 16.1, 15.0, 13.5, and 10.2 wt%, respectively (Table 1). The $d_{BJH}$ of SBA-15 was about 2 or 3 times larger than that of MCM-41, while the $C$ value of HDC-193/SBA-15 was just increased less than 3% points, indicating that the constraint of SBA-15 was weakened due to large pore diameter ($d_{BJH} = 6.39$ nm). There exists electrostatic interaction between HDC-193 molecules and the channel wall of modified mesoporous silica due to that HDC-193 is anion surfactant.

The $N_2$ adsorption/desorption isotherms and calculated pore diameter distribution of HDC-193/SBA-15 and

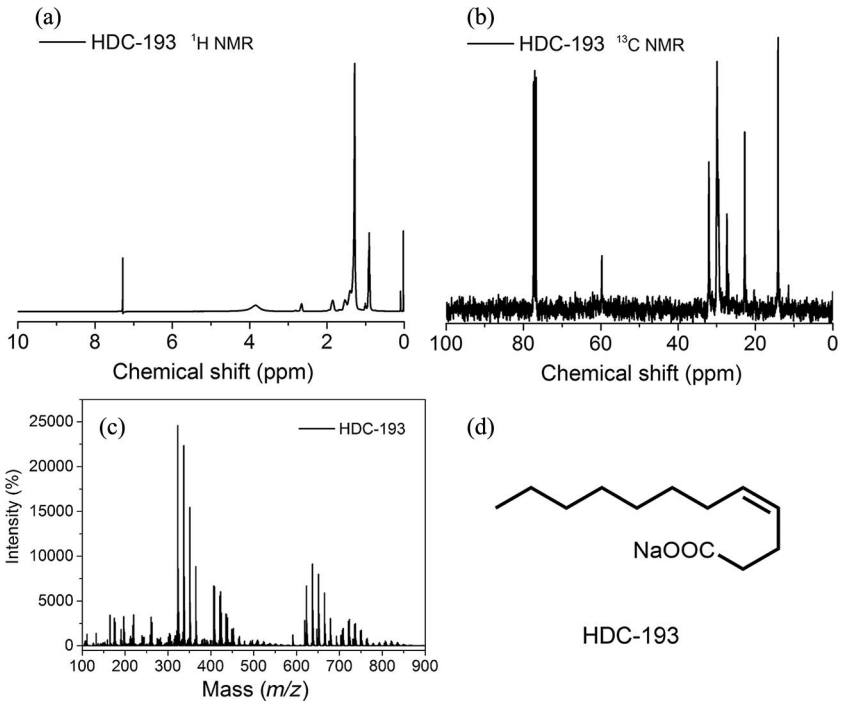


**Figure 2.** (a) $^{1}$H NMR, (b) $^{13}$C NMR, (c) MALDI-TOF MS spectra of HDC-193, and (d) molecular structure of HDC-193. *Note*: MALDI-TOF MS, matrix-assisted laser desorption/ionization time-of-flight mass spectrometry.

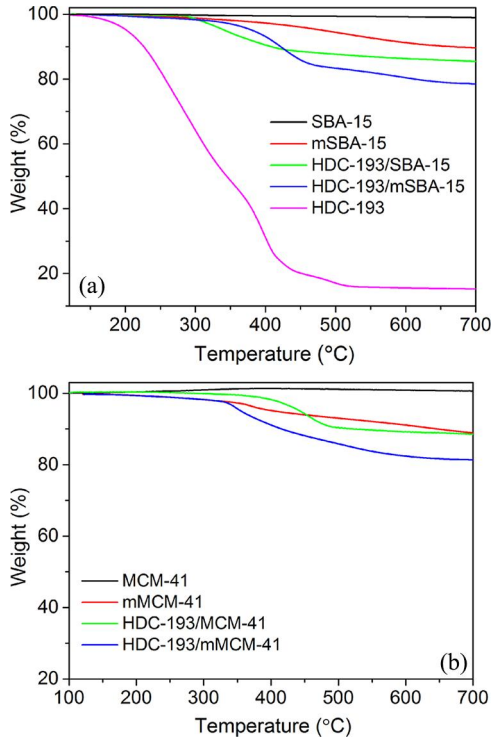


**Figure 3.** TGA curves of (a) SBA-15, mSBA-15, HDC-193, HDC-193/SBA-15, and HDC-193/mSBA-15; (b) MCM-41, mMCM-41, HDC-193/MCM-41, and HDC-193/mMCM-41. *Note*: TGA, thermogravimetric analysis.

**Table 1.** Effective HDC-193 uptake in different mesoporous silica.

| Samples | *C* (%) |
|---|---|
| HDC-193/SBA-15 | 16.1 |
| HDC-193/mSBA-15 | 15.0 |
| HDC-193/MCM-41 | 13.5 |
| HDC-193/mMCM-41 | 10.2 |

HDC-193/mSBA-15 are shown in Figure 4, respectively. Compared with SBA-15 and mSBA-15 (Figures 1c and 1d), the mesoporous structure of mesoporous silica was not broken, and the pore size was decreased by encapsulating SMS. Moreover, the decreased $d_{BJH}$ of HDC-193/SBA-15 and HDC-193/mSBA-15 indicated that the HDC-193 molecules entered into the channels of SBA-15 and mSBA-15.

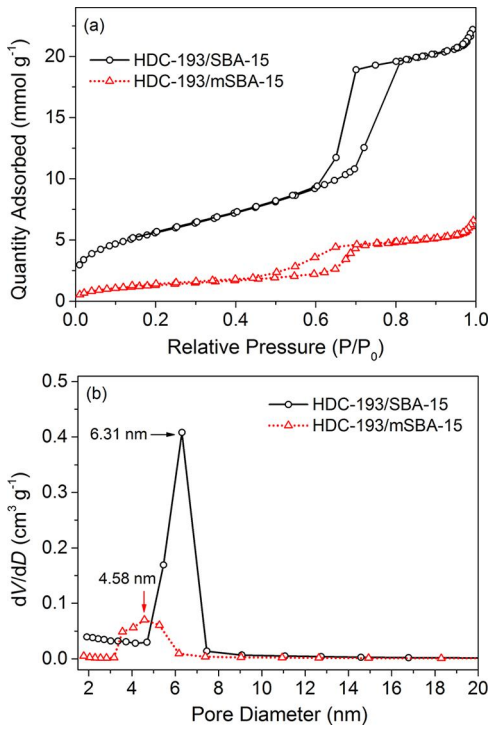


**Figure 4.** (a) $N_2$ adsorption/desorption isotherm and (b) pore diameter distribution of HDC-193/SBA-15 and HDC-193/mSBA-15.

### 3.4. Electrical conductivity of polystyrene composites

The electrical conductivity of PS composites were increased with a small amount of SMS (0.5–1.0 wt%) and became stable with the increasing SMS content. According to the Electronic Industries Association standards, conductive materials have a surface electrical resistivity $\rho_s$ of less than $1.0 \times 10^5\,\Omega\,sq^{-1}$, dissipative materials have a $\rho_s$ from $1.0 \times 10^5$ to $1.0 \times 10^{12}\,\Omega\,sq^{-1}$, and insulating materials have a $\rho_s$ higher than $1.0 \times 10^{12}\,\Omega\,sq^{-1}$ [47]. The HDC-193/PS composite with 0.3 wt% of HDC-193 had excellent antistatic property with $\rho_s$ value of $9.2 \times 10^{10}\,\Omega\,sq^{-1}$, and the $\rho_s$ decreased with the increasing HDC-193 content. When the HDC-193 content was higher than 1.0 wt%, the $\rho_s$ was not significantly decreased with further increasing HDC-193. Similar tendency was observed for the HDC-193/mSBA-15/PS composites (Figure 5a).

The $\rho_s$ of HDC-193/PS was lower than that of HDC-193/mSBA-15/PS with the same HDC-193 mass fraction (Figure 5a), which may be attributed to the increased surface roughness of HDC-193/mSBA-15/PS with the addition of mSBA-15. According to the research on super hydrophobic coating, to impart the super hydrophobicity on the surface, nanoparticles such as $SiO_2$, $TiO_2$, ZnO, and CNT can be introduced onto the surfaces to create nano scale roughness in addition to low surface energy, which had adverse effect on increasing the antistatic properties [48,49]. The hydrophobic mesoporous silica mSBA-15 on the surface of PS composite sheet can increase the roughness and hydrophobicity of the surface, resulting in decreased antistatic effect. As depicted in Figure 6, the surface roughness $R_q$ and $R_a$ of the HDC-193/mSBA-15/PS increased to more than 2-fold compared to HDC-193/PS. As a result, the $\rho_s$ of HDC-193/PS was lower than that of HDC-193/mSBA-15/PS when with the same HDC-193 content. The $\rho_s$ of MCM-41/PS with different mass fractions of MCM-41 was investigated, and the results showed that the $\rho_s$ was slightly increased with mass fraction of MCM-41 (Figure 5b).

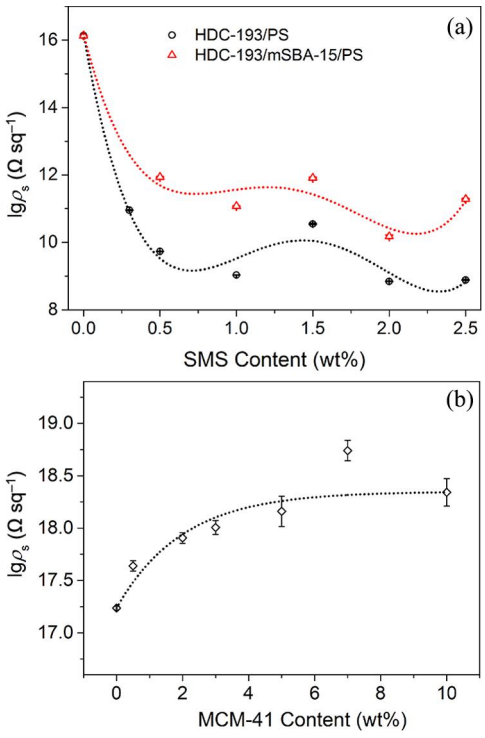


Figure 5. (a) $\rho_s$ vs. SMS content of HDC-193/PS and HDC-193/mSBA-15/PS; (b) $\rho_s$ vs. MCM-41 content of MCM-41/PS composites. *Note*: SMS, small molecular surfactant.

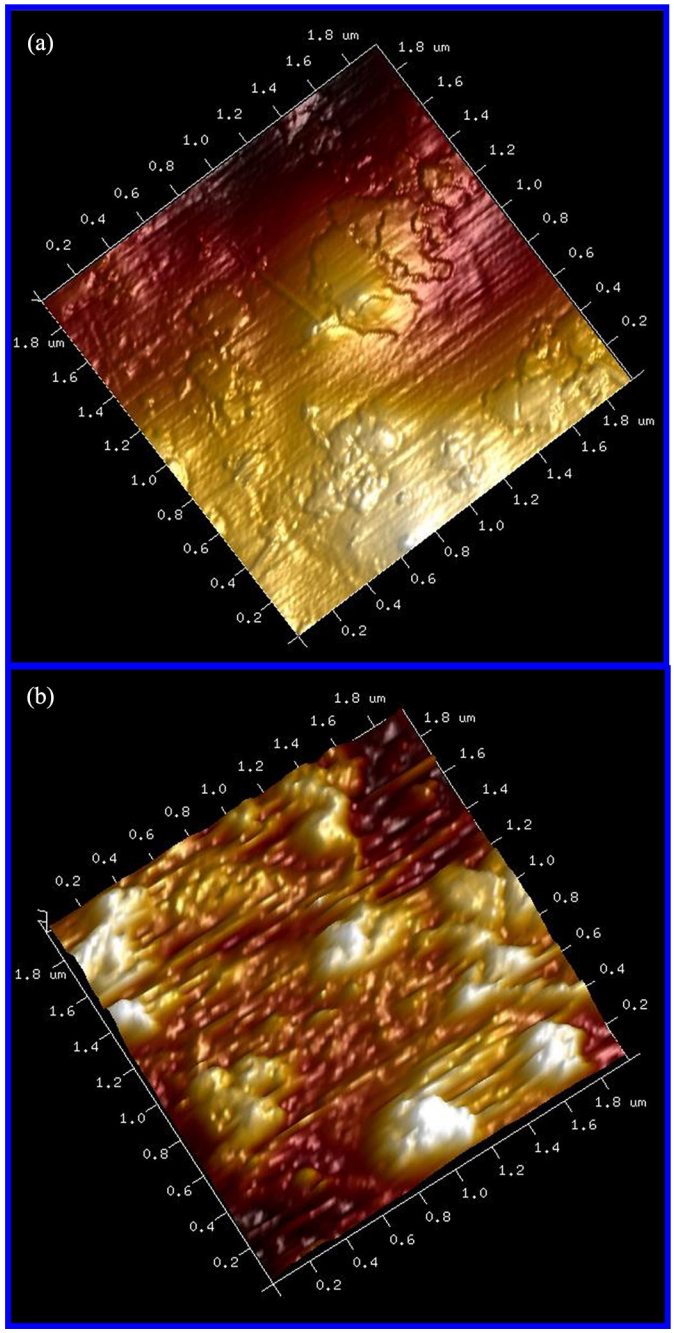


Figure 6. AFM results including the topographic images and roughness of the surface of (a) HDC-193/PS with $R_q = 8.0$ nm and $R_a = 6.4$ nm, (b) HDC-193/mSBA-15/PS with $R_q = 19.5$ nm and $R_a = 14.9$ nm. *Note*: AFM, atomic force microscopy.

The $\rho_s$ of PS composites was affected by varied factors, such as the content and molecular structures of SMS, the pore size, functional groups, and surface roughness of mesoporous silica. The PS composites with varied mesoporous silica were prepared and the $\rho_s$ values were compared to investigate the

**Table 2.** $\rho_s$ of PS composites with HDC-193 encapsulated in varied mesoporous silica.

| Samples | $\rho_s(\Omega\,sq^{-1})$ |
|---|---|
| HDC-193/SBA-15/PS | $6.4 \times 10^{13}$ |
| HDC-193/mSBA-15/PS | $8.2 \times 10^{11}$ |
| HDC-193/MCM-41/PS | $2.4 \times 10^{9}$ |
| HDC-193/mMCM-41/PS | $9.2 \times 10^{13}$ |

effects of pore size and functional groups of mesoporous silica on the $\rho_s$ values. The PS composites with encapsulated antistatic agents which contain 1.5 wt% of HDC-193 were taken as an example, and the results are shown in Table 2. The pore size of mSBA-15 was a little smaller than that of SBA-15, while HDC-193/mSBA-15/PS showed a $\rho_s$ of 2 order of magnitudes lower than that of HDC-193/SBA-15/PS, which can be resulted from the modification of SBA-15 by APTES. Introduction of APTES with amino groups on the surface of the mesoporous silica can create a hydrophilic microenvironment, and amino group can adsorb water molecules in the air to assist the formation of aqueous layer on the surface of PS composites. The MCM-41 was modified by APTES to prepare mMCM-41 which showed smaller pore size than that of MCM-41. The HDC-193/mMCM-41/PS composite showed higher $\rho_s$ of $9.2 \times 10^{13}\,\Omega\,sq^{-1}$ than that of HDC-193/MCM-41/PS composite, which may be attributed to the too small pore size of mMCM-41 and very low HDC-193 content in the channel of mMCM-41 (Table 2).

### 3.5. Sustained release effect of SMS encapsulated into mesoporous silica

The lifetime of SMS in the PS composites was related to the diffusion process of SMS from the matrix to the surface of composite products, which was affected by the SMS molecular structures, mesoporous structures, interaction between SMS and mesoporous silica, etc. It is supposed that encapsulating the SMS in the channel of mesoporous silica could decrease the diffusion rate of SMS from the matrix to the surface of products, and improving the interaction between SMS and mesoporous silica could further decrease the diffusion rate and prolong the lifetime of SMS in the PS composites.

To understand how the SMS molecules behave in the PS matrix and mesoporous silica channels, the root-mean-square displacement (RMSD) and diffusion coefficient $D_G$ of additive was analyzed (Figure 7). The RMSD of SMS in SMS/PS was 52.2 nm for 10 ps, while the RMSD in SMS/MSN/PS was obviously reduced, indicating that diffusion rate of SMS was decreased by encapsulating SMS in the channel of MSN. Comparing the RMSD in channels with different radii, the RMSD of SMS was decreased with the decreasing channel radius, indicating that smaller channel radius can effectively decrease the diffusion rate of SMS.

The SMS in SMS/MSN/PS composites showed three diffusion coefficients (Table 3), in which $D_{G1}$ represented the diffusion process in the channel, $D_{G2}$ represented diffusion from the channel to the PS matrix, and $D_{G3}$ represented diffusion from the matrix to the surface of composite, respectively. The $D_G$ of SMS in SMS/PS composite is $1.7 \times 10^{-8}\,m^2\,s^{-1}$. The $D_{G1}$ of SMS decreased with the decreasing radius of MSN, in which the $D_{G1}$ of SMS diffusion in the channels SMS/MSN/PS6, SMS/MSN/PS4, and SMS/MSN/PS2 is $1.0 \times 10^{-8}$, $0.9 \times 10^{-8}$, and $0.7 \times 10^{-8}\,m^2\,s^{-1}$, respectively. The $D_{G2}$ of SMS is $1.2 \times 10^{-8}$–$1.3 \times 10^{-8}\,m^2\,s^{-1}$, which is not affected by the decreasing radius of MSN. When the SMS diffused in the PS matrix, the $D_{G3}$ is $1.8 \times 10^{-8}$–$2.0 \times 10^{-8}\,m^2/s^{-1}$, which is a little higher than

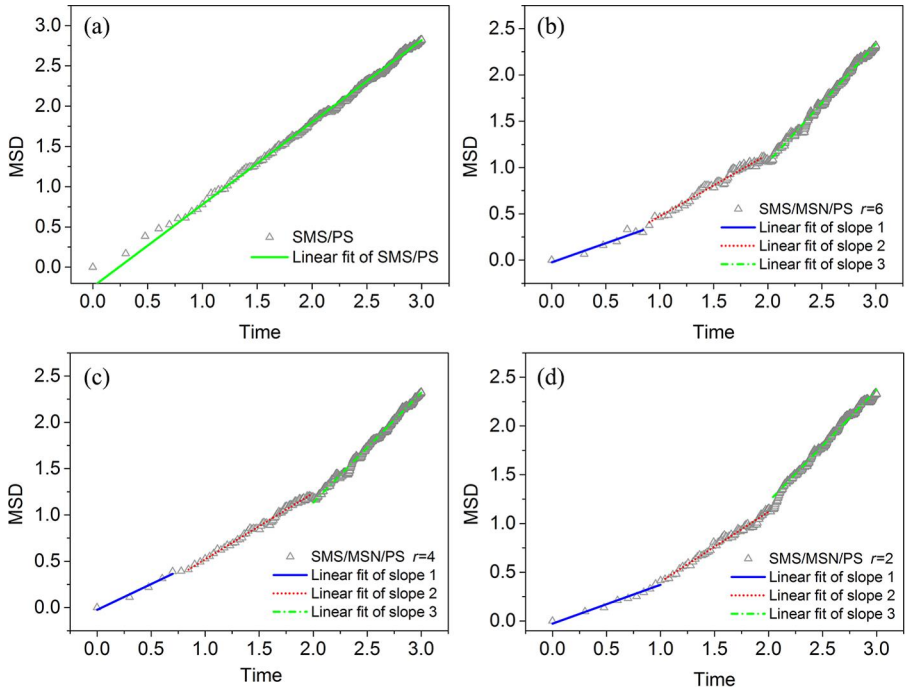


**Figure 7.** Mean-square displacement (MSD) vs. Time for SMS in (a) SMS/PS, (b–d) SMS/MSN/PS, $r = 6$, 4, and 2. *Note*: SMS, small molecular surfactant; MSN, mesoporous silica nanoparticle.

**Table 3.** Diffusion rate and RMSD of SMS in PS composites.

| Sample | $D_{G1}$ ($m^2\ s^{-1}$) | $D_{G2}$ ($m^2\ s^{-1}$) | $D_{G3}$ ($m^2\ s^{-1}$) | RMSD (nm) |
|---|---|---|---|---|
| SMS/MSN/PS6 | $1.0 \times 10^{-8}$ | $1.3 \times 10^{-8}$ | $1.8 \times 10^{-8}$ | 39.0 |
| SMS/MSN/PS4 | $0.9 \times 10^{-8}$ | $1.2 \times 10^{-8}$ | $2.0 \times 10^{-8}$ | 35.7 |
| SMS/MSN/PS2 | $0.7 \times 10^{-8}$ | $1.2 \times 10^{-8}$ | $1.9 \times 10^{-8}$ | 35.3 |

RMSD, root-mean-square displacement.

that of SMS/PS composite. The $D_{G1}$ and $D_{G2}$ in SMS/MSN/PS composites were lower than $D_G$ of SMS in SMS/PS composite due to the bound effect of channels, and the diffusion rate of SMS in small channel was lower than that of large channel radius.

### 3.6. Washing durability of polystyrene composites

The PS composites were washed in the deionized water by ultrasonication, and then the $\rho_s$ was tested to investigate the diffusion rate and the lifetime of SMS in the composites. The effective mass fraction of HDC-193 in PS composites was controlled as 1.0 wt% for testing the washing effect. The $\rho_s$ of HDC-193/PS composite after washing once was increased to $1.1 \times 10^{13}\ \Omega\ sq^{-1}$ (Figure 8), signifying a loss of the antistatic property. By comparison, the $\rho_s$ of HDC-193/SBA-15/PS composite after washing twice was $1.2 \times 10^{12}\ \Omega\ sq^{-1}$ and HDC-193/mSBA-15/PS composite after washing five times was $1.1 \times 10^{12}\ \Omega\ sq^{-1}$ (Figure 8), which retained weak antistatic property. This indicated that the lifetime of HDC-193/SBA-15/PS composite and HDC-193/mSBA-15/PS composite was much longer than that of HDC-193/PS composite, which was consistent with the simulation results of SMS diffusion process in SMS/PS and SMS/MSN/PS.

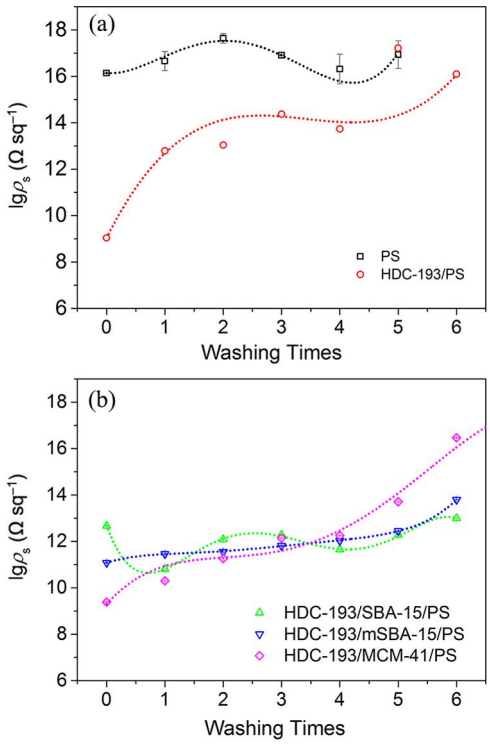


**Figure 8.** Surface electrical resistivity $\rho_s$ vs. Washing times of PS and its composites with 1.0 wt% of HDC-193.

The washing effect of PS sheet was also investigated as blank reference (Figure 8). The PS before and after washing retained nearly equal $\rho_s$ of $10^{16}$–$10^{17}\ \Omega\ sq^{-1}$, indicating that the washing effect of PS composites was not affected by PS matrix. The physical and chemical structures of mesoporous silica and antistatic agent were key factors to influence the washing effect of PS composites.

The washing effect of PS composites with HDC-193 encapsulated in various mesoporous silica was investigated to declare the effect of channel radius (pore diameter) on the diffusion rate of HDC-193 from the inner channel to the surface of PS composite sheet (Figure 8a). The channel diameter of SBA-15 were larger than that of mSBA-15 according to Figures 1c and 1d, resulting in quick release of HDC-193 from the inner channel of SBA-15. The surface electrical resistivity $\rho_s$ of HDC-193/SBA-15/PS composite after washing twice was $1.2 \times 10^{12}\ \Omega\ sq^{-1}$, which was higher than that of HDC-193/mSBA-15/PS ($3.5 \times 10^{11}\ \Omega\ sq^{-1}$) and HDC-193/MCM-41/PS ($1.8 \times 10^{11}\ \Omega\ sq^{-1}$). The results indicated that the diffusion rate of HDC-193 in mesoporous silica with large channel radius was quicker than that of mesoporous silica with small channel radius. The $\rho_s$ of HDC-193/MCM-41/PS composite after washing thrice was $1.4 \times 10^{12}\ \Omega\ sq^{-1}$, which was higher than that of HDC-193/mSBA-15/PS ($6.4 \times 10^{11}\ \Omega\ sq^{-1}$), though the channel radius of MCM-41 was smaller than that of mSBA-15 (Figure 8b). The increased washing resistance of PS composite with mSBA-15 may be attributed to the functional groups of mSBA-15 which had strong interaction with HDC-193 to reduce the diffusion rate of HDC-193 from the inner channel to the surface of PS composite sheet.

The sustained release mechanism of SMS was concluded from previous studies [30] and MD simulation in this work. The results showed that the SMS molecules first go through the long-range order channel structure arrangement in MSN and then migrate to the PS composite surface. Moreover, the SMS molecules should keep away from MSN distributed in the PS matrix during their migration procedure. As a result, the SMS molecules encapsulated in MSN take longer time and need higher thermodynamic driving force to complete the migration procedure, compared to the SMS molecules without being encapsulated in MSN.

To further decrease the diffusion rate of SMS and prolong the lifetime of antistatic agents, the surface of the channel wall was organically modified with amino groups which has electrostatic host–guest interaction with anionic surfactant HDC-193. The electrostatic interaction induces the partial retention of HDC-193 on the silica walls surrounding the ordered array of mesoporous [42,50]. Similarly, the electrostatic interaction between amino groups outside the surface of SBA-15 and anions in HDC-193 molecules may also decrease the diffusion rate of HDC-193 from PS matrix to the surface of composite surface.

## 4. Conclusion

The antistatic agent HDC-193 has been loaded in mesoporous silica and APTES-modified mesoporous silica to design a controlled antistatic agents' delivery system, which may

prolong the lifetime of antistatic effect. The surface electrical resistivity $\rho_s$ of HDC-193/PS was lower than that of HDC-193/mSBA-15/PS when with the same HDC-193 content, which may be attributed to the increased surface roughness of HDC-193/mSBA-15/PS with the addition of mSBA-15. The HDC-193/mSBA-15/PS showed a $\rho_s$ of 2 order of magnitudes lower than that of HDC-193/SBA-15/PS. The reason is that the amino groups on the surface of SBA-15 can create a hydrophilic microenvironment and thus adsorbing water molecules in the air to assist the formation of aqueous layer on the surface of PS composites.

The MD simulation predicted that the diffusion rate of SMS was reduced due to the encapsulation in the channel of mesoporous silica and decreased with the channel diameter. The reduced diffusion rate resulted in a long lifetime of SMS in PS composites, which was confirmed by the washing results. The modification of SBA-15 further reduced the diffusion rate of HDC-193 and resulted in even longer lifetime of HDC-193/mSBA-15/PS than that of HDC-193/SBA-15/PS and HDC-193/MCM-41/PS.

## Funding

The authors thank the financial support from the National Natural Science Foundation of China (Grant Nos. 21374023 and 21574027). The authors thank also the financial support from the Open Project Foundation of State Key Laboratory of Molecular Engineering of Polymers (Fudan University) (Grant No. K2017-19), and The Basic Scientific Research Project of Central University (Grant No. 2017B00614).

## References

[1] Greason, W. D. *IEEE Trans. Ind. Appl.* **1987**, *IA-23*, 205–216.
[2] Gibson, N. *J. Electrost.* **1997**, *40–41*, 21–30.
[3] Lai, S. T. *Overview of Surface and Deep Dielectric Charging on Spacecraft*; Spacecraft Charging, Progress in Astronautics and Aeronautics, 2011; pp. 1–17.
[4] Angelopoulos, M. *IBM J. Res. Dev.* **2001**, *45*, 57–75.
[5] Baytekin, H. T.; Baytekin, B.; Incorvati, J. T.; Grzybowski, B. A. *Angew. Chem. Int. Ed.* **2012**, *51*, 4843–4847.
[6] Baytekin, H. T.; Baytekin, B.; Hermans, T. M.; Kowalczyk, B.; Grzybowski, B. A. *Science* **2013**, *341*, 1368–1371.
[7] Burgo, T. A.; Ducati, T. R.; Francisco, K. R.; Clinckspoor, K. J.; Galembeck, F.; Galembeck, S. E. *Langmuir* **2012**, *28*, 7407–7416.
[8] Williams, M. W. *AIP Adv.* **2012**, *2*, 010701.
[9] Baytekin, B.; Baytekin, H. T.; Grzybowski, B. A. *J. Am. Chem. Soc.* **2012**, *134*, 7223–7226.
[10] Bhandari, H.; Bansal, V.; Choudhary, V.; Dhawan, S. K. *Polym. Int.* **2009**, *58*, 489–502.
[11] Qaiser, A. A.; Hyland, M. M.; Patterson, D. A. *J. Phys. Chem. B* **2011**, *115*, 1652–1661.
[12] De, S.; King, P. J.; Lyons, P. E.; Khan, U.; Coleman, J. N. *ACS Nano* **2010**, *4*, 7064–7072.
[13] Krupa, I.; Cecen, V.; Boudenne, A.; Prokeš, J.; Novák, I. *Mater. Des.* **2013**, *51*, 620–628.
[14] Aal, N. A.; El-Tantawy, F.; Al-Hajry, A.; Bououdina, M. *Polym. Compos.* **2008**, *29*, 125–132.
[15] Rhodes, S. M.; Higgins, B.; Xu, Y.; Brittain, W. J. *Polymer* **2007**, *48*, 1500–1509.
[16] Wang, H.; Xie, G.; Fang, M.; Ying, Z.; Tong, Y.; Zeng, Y. *Compos. Part B Eng.* **2015**, *79*, 444–450.
[17] Martins, C. R.; De Paoli, M.-A. *Eur. Polym. J.* **2005**, *41*, 2867–2873.
[18] Omastova, M.; Chodak, I.; Pionteck, J. *Synth. Metals* **1999**, *102*, 1251–1252.
[19] He, M.; Han, W.; Ge, J.; Yang, Y.; Qiu, F.; Lin, Z. *Energy Environ. Sci.* **2011**, *4*, 2894–2902.
[20] He, M.; Ge, J.; Lin, Z.; Feng, X.; Wang, X.; Lu, H.; Yang, Y.; Qiu, F. *Energy Environ. Sci.* **2012**, *5*, 8351–8358.
[21] Zheng, A.; Xu, X.; Xiao, H.; Li, N.; Guan, Y.; Li, S. *Appl. Surf. Sci.* **2012**, *258*, 8861–8866.
[22] Chow, W.; Tham, W. *eXPRESS Polym. Lett.* **2009**, *3*, 116–125.
[23] Grob, M. C.; Minder, E. *Plast. Addit. Compd.* **1999**, *1*, 20–26.
[24] Ghosh, P.; Chakrabarti, A. *Eur. Polym. J.* **2000**, *36*, 1043–1054.
[25] Pantea, D.; Darmstadt, H.; Kaliaguine, S.; Sümmchen, L.; Roy, C. *Carbon* **2001**, *39*, 1147–1158.
[26] Schwarz, M.-K.; Bauhofer, W.; Schulte, K. *Polymer* **2002**, *43*, 3079–3082.
[27] Nam, S.; Cho, H. W.; Lim, S.; Kim, D.; Kim, H.; Sung, B. J. *ACS Nano* **2012**, *7*, 851–856.
[28] Li, C.; Liang, T.; Lu, W.; Tang, C.; Hu, X.; Cao, M.; Liang, J. *Compos. Sci. Technol.* **2004**, *64*, 2089–2096.
[29] Shyr, T.-W.; Lien, C.-H.; Lin, A.-J. *Text. Res. J.* **2011**, *81*, 254–263.
[30] Li, R.; Si, J.; Tang, P. *Polym. Adv. Technol.* **2016**, *27*, 615–622.
[31] Wang, Z. W.; Wang, P. L.; Hu, C. Y. *Pack. Technol. Sci.* **2012**, *25*, 329–339.
[32] Gillet, G.; Vitrac, O.; Desobry, S. *Ind. Eng. Chem. Res.* **2010**, *49*, 7263–7280.
[33] Alin, J.; Hakkarainen, M. *J. Appl. Polym. Sci.* **2010**, *118*, 1084–1093.
[34] Bertoldo, M.; Ciardelli, F. *Polymer* **2004**, *45*, 8751–8759.
[35] Skoulidas, A. I.; Bowen, T. C.; Doelling, C. M.; Falconer, J. L.; Noble, R. D.; Sholl, D. S. *J. Membr. Sci.* **2003**, *227*, 123–136.
[36] Ahn, W.-Y.; Kalinichev, A. G.; Clark, M. M. *J. Membr. Sci.* **2008**, *309*, 128–140.
[37] Russell, R.; Axel, A.; Shields, K.; Pishko, M. *Polymer* **2001**, *42*, 4893–4901.
[38] Bemporad, D.; Essex, J. W.; Luttmann, C. *J. Phys. Chem. B* **2004**, *108*, 4875–4884.
[39] Xiang, T.-X.; Anderson, B. D. *Adv. Drug Deliv. Rev.* **2006**, *58*, 1357–1378.
[40] Murad, S. *J. Chem. Phys.* **2011**, *134*, 114504.
[41] Zhang, J.; Qiao, Z. A.; Mahurin, S. M.; Jiang, X.; Chai, S. H.; Lu, H.; Nelson, K.; Dai, S. *Angew. Chem.* **2015**, *127*, 4665–4669.
[42] Wan, M. M.; Yang, J. Y.; Qiu, Y.; Zhou, Y.; Guan, C. X.; Hou, Q.; Lin, W. G.; Zhu, J. H. *ACS Appl. Mater. Interf.* **2012**, *4*, 4113–4122.
[43] Weng, C. J.; Chen, Y. L.; Jhuo, Y. S.; Lin, Y. L.; Yeh, J. M. *Polym. Int.* **2013**, *62*, 774–782.
[44] Pham, V. H.; Cuong, T. V.; Dang, T. T.; Hur, S. H.; Kong, B. S.; Kim, E. J.; Shin, E. W.; Chung, J. S. *J. Mater. Chem.* **2011**, *21*, 11312–11316.
[45] Cai, Q.; Luo, Z. S.; Pang, W. Q.; Fan, Y. W.; Chen, X. H.; Cui, F. Z. *Chem. Mat.* **2001**, *13*, 258–263.
[46] Nan, C. W.; Fan, L. Z.; Lin, Y. H.; Cai, Q. *Phys. Rev. Lett.* **2003**, *91*, 4.
[47] Phuchaduek, W.; Rattanasak, U.; Kaewpirom, S. *Songklanakarin J. Sci. Technol.* **2013**, *35*, 529–535.
[48] Fu, Q.; Wu, X.; Kumar, D.; Ho, J. W.; Kanhere, P. D.; Srikanth, N.; Liu, E.; Wilson, P.; Chen, Z. *ACS Appl. Mater. Interf.* **2014**, *6*, 20685–20692.
[49] Kwon, S. O.; Park, C. H.; Kim, J. *J. Eng. Fiber Fabr.* **2015**, *10*, 46–56.
[50] Balas, F.; Manzano, M.; Horcajada, P.; Vallet-Regí, M. *J. Am. Chem. Soc.* **2006**, *128*, 8116–8117.